LOng-LIved greenhouse gas PrOducts Performances (LOLIPOP)

WP3300 - Monitoring of stratospheric chlorine levels and their impacts on ozone recovery

D3.2.3 - User Case Study Technical Note

Document Reference	[D3.1] LOLIPOP_UCS-FR_v1.1
Document Authors	Dr Antonio G. Bruno Dr Jeremy J. Harrison Dr Sandip S. Dhomse Prof Martyn P. Chipperfield
Document Approvers	S. Pinnock (ESA, Technical Officer)

Change log:

Version Nr.	Date	Status	Reason for change
Version 1.0	15-11-2025	First submission of the document	N/A
Version 1.1	26-02-2026		Minor corrections to address ESA RIDs

Table of Contents

1 Introduction/Scientific background

The 1987 Montreal Protocol (MP) and its later amendments introduced the legal framework for controlling production of and phasing out ozone-depleting substances (ODSs) including halogen source gases such as chlorofluorocarbons (CFCs) and hydrochlorofluorocarbons (HCFCs) (WMO, 2023). More recently hydrofluorocarbons (HFCs) have been included, although these do not deplete stratospheric ozone, but are only present in the atmosphere as CFC or HCFC replacements. As well as being sources of atmospheric halogens, CFCs, HCFCs and HFCs are very strong greenhouse gases (GHGs). Most of the controlled halogen source gases have long atmospheric lifetimes (decades or more) and degrade via reaction with OH or photolysis in the stratosphere, forming reservoir species, the most abundant being hydrogen chloride (HCl) and hydrogen fluoride (HF). The monitoring of all these species is essential in order to evaluate the success of the MP, in particular HCl, for which the most abundant halogen source gases are the CFCs and HCFCs. Accurate observations of the source gases and reservoir species throughout the upper troposphere – stratosphere profile can provide an important constraint on deriving the budget of the main halocarbon GHGs.

Due to its long data record (since 2004) and sensitivity to the stratosphere, Atmospheric Chemistry Experiment – Fourier Transform Spectrometer (ACE-FTS) (Schmidt et al., 2024) observations are essential to monitor the key chlorine/fluorine source gases, such as CFC-11 and CFC-12, and reservoir species, such as HCl and HF. Satellite data in combination with atmospheric models are also useful to evaluate the role of these species in ozone depletion. The TOMCAT global 3-D model (Chipperfield, 2006) has been widely used to evaluate the observations of ozone depleting substances in the atmosphere and determine their impact on the ozone levels, and to diagnose the variation in the extent of stratospheric ozone depletion.

To overcome the problem of gaps in the satellite sampling, Dhomse and Chipperfield (2023) have constructed long-term, gap-free atmospheric profile datasets using data assimilation based on a supervised machine learning (ML) scheme, the eXtreme Gradient Boost (XGBoost) regression model. Using this scheme, it has been possible to create HCl and HF datasets extending back to 1991 using data from multiple instruments like ACE-FTS and the HALogen Occultation Experiment (HALOE). The ML-derived datasets for CFC-11 and CFC-12 extend back to 2000, although ACE-FTS data is available from February 2004.

2 Approach/Methods

2.1 Instruments/models/techniques description

The aim of WP3300 is to study stratospheric chlorine levels over recent decades and their impacts on ozone recovery. To this end, we have used a combination of direct observations, atmospheric modelling, and machine-learning-based datasets. This work will also inform the potential for stratospheric halogen observations to help constrain budgets of CFC, HCFC and HFC emissions.

The principal observational dataset comprises vertical profiles of trace gas mixing ratios measured by the ACE-FTS limb instrument, onboard the Canadian satellite SCISAT, which operates in a solar occultation viewing geometry (Bernath, 2017, 2005). ACE has been providing measurements of over 40 atmospheric trace gases, including HCl, HF, and many halogenated source gases, together with temperature and pressure. The long-term ACE time series, its high vertical resolution (3-4 km), and spectral resolution (0.02 cm^{-1} in the 750-4400

cm^{-1} region) allows for a comprehensive analysis of stratospheric variability during the last decades. Here we make use of the recent v5.2 data product.

We use outputs from TOMCAT, an off-line three-dimensional (3D) global chemical transport model, which uses winds and temperatures from meteorological analyses (i.e., ECMWF ERA5.1) to specify the atmospheric transport and temperature, and calculates the vertical profile and abundance of chemical species in the troposphere and stratosphere. The model contains a comprehensive chemistry scheme for the stratosphere and has been used widely in the past to help interpret observations of ozone depleting substances in the atmosphere, and to diagnose the extent of stratospheric ozone depletion (Chipperfield et al., 2018; Feng et al., 2021; Hossaini et al., 2015).

We also make use of novel TCOM datasets. These are new datasets of chlorine and fluorine species produced using a data correction scheme based on extreme gradient boosting (XGBoost), a supervised machine learning algorithm. These datasets make use of TOMCAT simulations collocated with ACE-FTS measurements (Dhomse and Chipperfield, 2023) to produce gap-free profiles, with reduced biases and a better representation of seasonal variability.

In this report we investigate atmospheric trends of halogenated species using the technique of empirical mode decomposition (EMD), a data adaptive multi-resolution technique used to decompose signals into physically meaningful components (Huang et al., 1998). EMD is particularly suitable for the analysis of non-linear and non-stationary signals by separating these into components.

Unlike other decomposition techniques such as Fourier and wavelet, the EMD technique is an empirical method developed to decompose time series properties through an iterative process into a sequence of mono-component signals known as intrinsic mode functions (IMFs). It consists of five main steps:

I. identification of the local extrema of the signal *x(t)*;
II. interpolation of the local extrema obtaining the envelopes of the minima and the maxima;
III. determination of the mean signal *m(t)* between the two envelopes;
IV. determination of the first residual $d_1(t)$ as the difference between the signal and *m(t)*; $d_1(t)$ is considered an IMF if it satisfies two conditions: the number of local extrema and of zero crossings points does not differ by more than one and the mean value of the envelopes is zero at any point;
V. if $d_1(t)$ does not meet the conditions, the sifting process is repeated using $d_1(t)$ as the original signal, producing a new candidate to be an IMF.

When calculating EMD two problems can be present:

- “mode mixing” or “mode splitting”, respectively the presence of more than one mode in an IMF or the splitting of a mode in more than one IMF
- the distortion of the signal at the boundaries.

To prevent mode mixing (or splitting), we decided to use a noise-assisted EMD approach, the Complete Ensemble Empirical Mode Decomposition with Adaptive Noise (CEEMDAN) (Colominas et al., 2014; Torres et al., 2011). It is based on the Ensemble Empirical Mode Decomposition (EEMD) strategy of adding noise to observations (Li et al., 2010) introducing adaptive noise in the recursive IMF extraction. The CEEMDAN steps are:

I. create an ensemble of noisy signals by adding Gaussian noise $w_i(t)$ to the original timeseries $x(t)$

$$x_i'(t) = x(t) + w_i(t);$$

II. apply Empirical Mode Decomposition (EMD) to each noisy signal to obtain the first Intrinsic Mode Function (IMF),

$$d_{1,i} = EMD_1\big(x'_i(t)\big),$$

then compute the ensemble average of all first IMFs,

$$c_1(t) = \frac{1}{N}\sum_{i=1}^{N} d_{1,i}(t);$$

III. subtract the averaged first IMF from the original signal to determine the first residual,

$$r_1(t) = x(t) - c_1(t);$$

IV. add adaptive white noise $h_{k,i}(t)$ to each residual for subsequent IMFs,

$$r_{k,i}(t) = r_k(t) + h_{k,i}(t),$$

where $h_{k,i}(t)$ is adjusted to match the characteristics of the IMF being extracted;

V. obtain the k*th* IMF from each noisy residual using EMD and average across all ensemble members,

$$c_{k*1}(t) = \frac{1}{N}\sum_{i=1}^{N} EMD_k(r_{k,i}(t));$$

VI. repeat the above steps until the final residual becomes a monotonic function.

The CEEMDAN method enhances EEMD by ensuring signal completeness – the sum of all IMFs and the final residual exactly reconstructs the original signal – and by providing better IMF separation.

Like any signal processing technique, EMD and its derivations are sensitive to changes in boundary conditions. To reduce errors related to the signal boundaries the signal was right- and left-extended and forced to be periodic at the boundaries of the extended signal. The signal extension was performed in four steps:

I. subtraction of the mean from the signal;
II. symmetric extension of the results outside the boundaries to obtain a new signal five times longer (top panel Figure 1);
III. multiplication of the extended signal with a super-Gaussian window function which is equal to one in the original signal interval and smoothly decrease to zero at its edges (middle panel Figure 1);
IV. addition of the mean to the resulting signal (bottom panel Figure 1).

The resulting signal is periodic at the boundaries, and the boundary errors are reduced (Stallone et al., 2020).

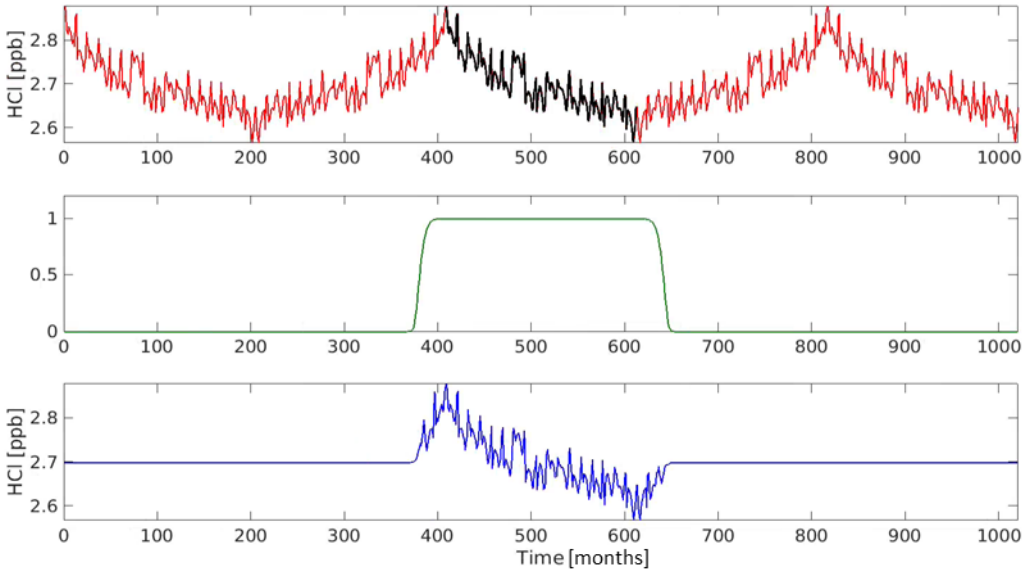

Figure 1. (Top panel) Example of HCl concentration extended signal in red and the original signal in black. (Middle panel) Super-Gaussian windowing function with exponent p=10. (Bottom panel) Final extended, periodic signal at the boundaries.

2.2 Input data description

ACE-FTS v5.2 profiles of HCl, CFC-11 and CFC-12 on a 1-km vertical grid from the surface up to 150 km have been used over the period 2004-2024. The retrieval range for each species is reported in Table 1. More details on the v5.2 retrieval scheme can be found in Boone et al. (2023) and Schmidt et al. (2024).

Table 1. Altitude range of the ACE-FTS v5.2 retrievals of HCl, CFC-11 and CFC-12.

Species	Lower altitude (km)	Upper altitude (km)
HCl	7	63
CFC-11	5	28
CFC-12	5	35

Because of its viewing geometry based on solar occultation, ACE measurements are sparse and the time series contain a number of gaps that can create errors in the signal decomposition when using the EMD technique. To reduce errors arising from these gaps, the ACE data have been interpolated using cubic splines. Figure 2 shows the comparison between the measured HCl averaged zonal means in an altitude band at 28.5-48.5 km and the same zonal means interpolated using cubic splines.

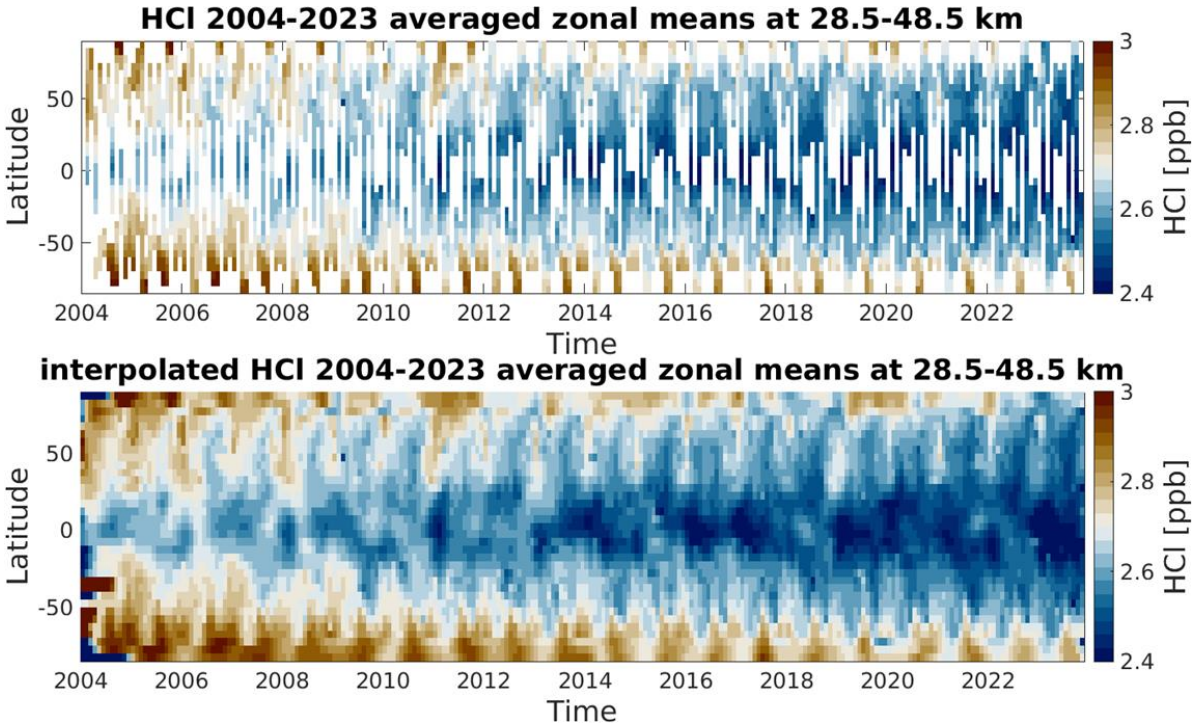

Figure 2. Measured (top panel) and interpolated (bottom panel) averaged HCl ACE zonal means at 28.5-48.5 km.

TOMCAT model simulations are performed at 2.8° horizontal resolution on 32 hybrid sigma-pressure levels from the surface to about 60 km. The model source gases are constrained by specifying the monthly global mean surface mixing ratios at the lowest model level. Although the model is forced by 6-hourly ECMWF ERA5 meteorology, the long-lived source gases are assumed to be well-mixed in the troposphere. These data are based on global surface networks (WMO, 2023). The outputs are available for 2000-2024 time period.

TCOM datasets of HCl (Dhomse, 2026), CFC-11 (Dhomse, 2026a), and CFC-12 (Dhomse, 2026b) on a 1-km vertical grid between 10 and 60 km have been used over the period 2000-2023 for CFC-11 and CFC-12, and 1991-2021 for HCl (Dhomse and Chipperfield, 2026, 2023). The TOMCAT simulations performed to produce these TCOM datasets were also performed at 2.8° resolution using the algorithm assimilated ACE-FTS data for CFC-11 and CFC-12, and ACE-FTS and HALOE data for HCl. The use of the ACE-FTS data helps to constrain biases between the model and observations and will also impose any additional variability observed.

3 Results

The HCl, CFC-11 and CFC-12 global trends have been evaluated for each of the three datasets used and the de-seasonalisation of the signal has been performed using the EMD-based method described in Section 2.1, allowing the identification and removal of the seasonal/annual cycle from the data. The trends in the concentrations of the observed species have been investigated using four approaches:

I. the analysis of trends calculated as the linear regression of the de-seasonalised cross sections over the period 2005-2024;
II. the analysis of the changes in the linear trends of the de-seasonalised averaged concentrations over some specific atmospheric regions.
III. the analysis of the nonlinear residuals of the decomposition via calculation of the first derivative to evaluate enhancement rates.
IV. the use of bespoke TOMCAT model simulations, a control run with the observed decreasing chlorine and a new run with constant Cl at peak values (1995) to evaluate the impact of the calculated trends of the reservoir species HCl.

3.1 Global trends

Figure 3 compares the cross-sectional trends of HCl, CFC-11, and CFC-12 derived from the ACE-FTS, TOMCAT, and TCOM datasets over the period 2005–2024 for CFCs. Overall, the trends calculated from the three datasets show good agreement, confirming the consistency between the observational (ACE-FTS) and model-based (TOMCAT and TCOM) estimates. For HCl, all datasets exhibit a clear negative trend throughout most of the stratosphere, particularly between 20 and 45 km, reflecting the ongoing decline in stratospheric chlorine due to reduced halocarbon emissions. The TOMCAT and TCOM simulations closely reproduce the observed spatial pattern and magnitude of the ACE-FTS trends, though with slightly smoother structures due to model resolution. For CFC-11 and CFC-12, negative trends dominate in the lower stratosphere, consistent with the gradual decrease in these compounds following the implementation of the Montreal Protocol. CFC-11 observation-based trends span a larger range of values than the ones calculated from the models due to a higher variability at high altitudes over polar regions. Minor regional differences appear in the magnitude and vertical extent of the trends, especially over the tropics and at high latitudes. Overall, the strong correspondence among the three datasets reinforces the robustness of the derived halocarbon trends and supports the reliability of both the model simulations and the observational analysis.

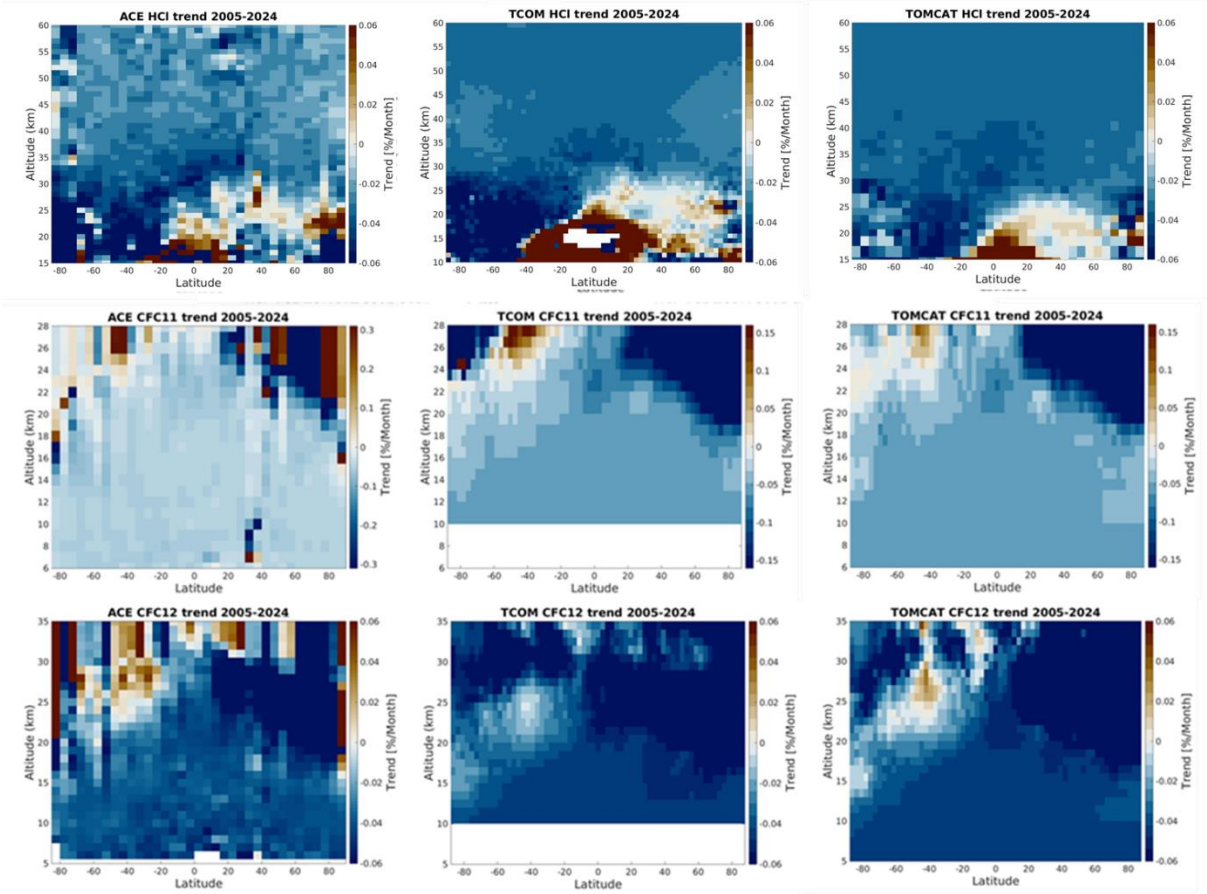

Figure 3. (Top row) Cross-sectional HCl trends between 2005 and 2021 for ACE-FTS (left), TOMCAT (middle) and TCOM (right). (Central row) Cross-sectional CFC-11 trends between 2005 and 2024. (Bottom row) Cross-sectional CFC-12 trends between 2005 and 2024. Note that ACE CFC-11 cross-sectional trends are reported using a different colour scale for a better visibility of the spatial patterns.

3.2 Averaged trends

The regions used to calculate the trends of the averaged VMRs are defined following Schmidt et al. (2024) to enable a comparison between analyses. For HCl the analysis covers altitudes between 28.5 and 48.5 km and latitudes from 60°S to 60°N, while for the CFCs it spans altitudes between 17.5 and 28.5 km and latitudes from 30°S to 30°N. The same study also provides the definition of the corresponding breaking points.

In the case of the CFCs the region chosen is at a higher altitude than used in Schmidt et al. (2024) so as not to include the troposphere; this is because the current setup of TOMCAT has fewer tropospheric levels and assumes that long-lived tracers are uniformly mixed throughout the troposphere. Hence, there is very little variability in the tracer concentrations that are averaged below tropopause altitudes (e.g. below 16 km in the tropics).

The study of atmospheric trends allows us to identify and highlight break points separating time periods with different trends, often associated with specific events. Examples are the slowdown of the Northern Hemisphere's atmospheric circulation in 2009 (e.g. Mahieu et al.,

2014), as illustrated in Figure 4 by the reduction in the loss rate of global stratospheric HCl, or the renewed CFC-11 emissions in China (Montzka et al., 2018) with a change in the loss rate in 2016-2020, and the return to a high reduction rate after 2020 in lower stratospheric CFC-11 (Figure 5). As expected, all three datasets show very similar decreasing trends for the three analysed species, as shown in Figures Figure 4-Figure 6 and summarised in Tables Table 2-Table 4.

The trends derived from the ACE-FTS, TOMCAT, and TCOM datasets show good overall agreement with those reported by Schmidt et al. (2024), confirming the general consistency among the different datasets. For HCl (Table 2), all datasets display a marked decrease during both analysed periods, with stronger negative slopes between 2005–2008 than between 2009–2021, indicating a slowdown in the decline rate over time. The ACE-FTS-based trends are slightly lower in magnitude than those from TOMCAT and TCOM but remain within their respective uncertainties. For CFC-11 (Table 3), the three datasets capture similar temporal behaviour, with a moderate decline from 2005–2014, a partial slowdown between 2015–2019 due to the renewed CFC emissions in China, and an accelerated decrease again after 2019. The ACE-FTS and TCOM results are particularly close to those reported by Schmidt and NOAA, while TOMCAT tends to show slightly smaller amplitudes. For CFC-12 (Table 4), all datasets reveal a clear transition from a weaker decline in 2005–2012 to a much steeper negative trend after 2013. Here again, TOMCAT and TCOM reproduce the Schmidt and NOAA trends well, though ACE-FTS exhibits slightly larger magnitudes. The larger discrepancy observed during the 2005–2012 period may be due to the non-linear decrease in the averaged CFC-12 VMR, which makes it more difficult to accurately extract a linear trend. Overall, the three species consistently show decreasing trends, and despite minor differences among the datasets, their temporal evolution and trend magnitudes are in strong agreement.

Table 2. HCl trends from Schmidt et al. (2024) and calculated from ACE-FTS, TOMCAT and TCOM datasets using the method described in Section 2.1.

	Slope 2005-2008 [ppt/yr]	Slope 2009-2024 [ppt/yr]
ACE v5.2 (Schmidt)	-20.86 ± 2.66	-8.64 ± 0.32
ACE v5.2	-14.64 ± 4.09	-8.50 ± 4.09
TOMCAT	-18.82 ± 5.13	-9.57 ± 1.33
TCOM	-20.86 ± 3.14	-8.9 ± 1.01

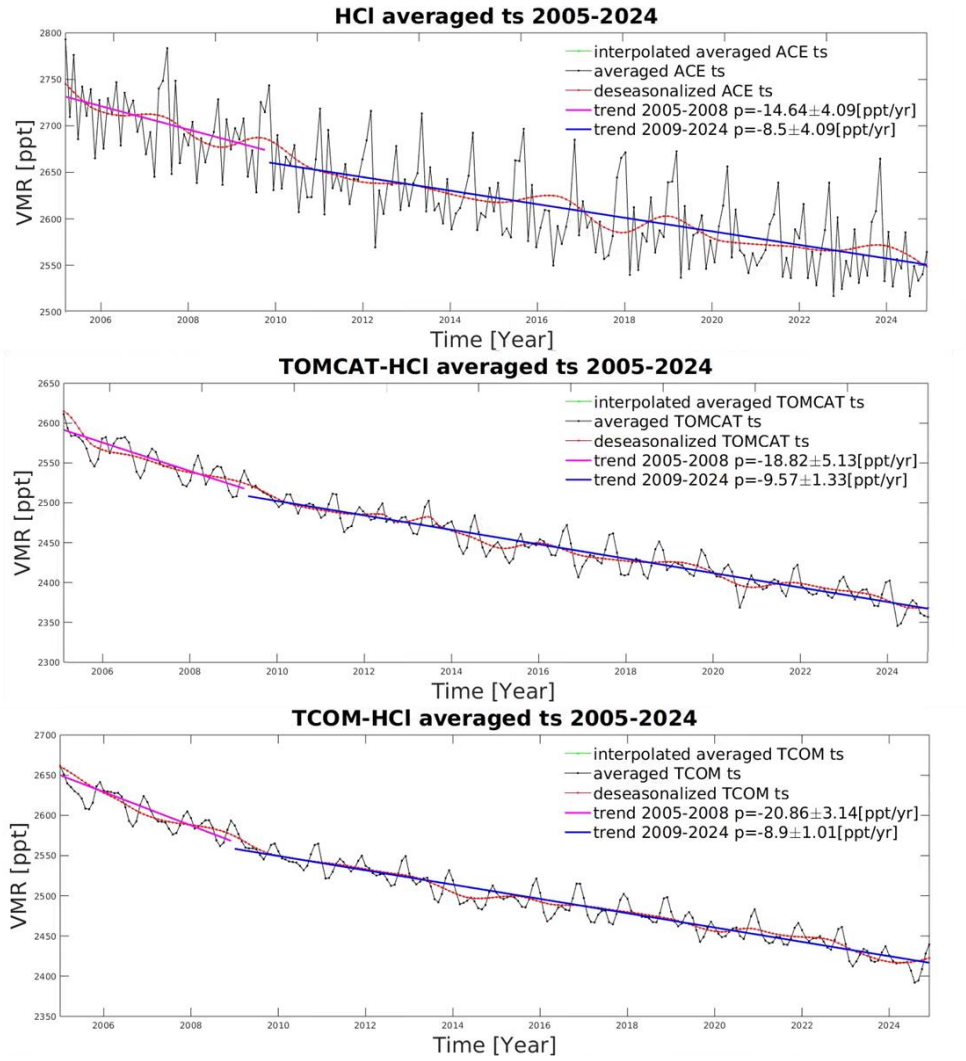

Figure 4. HCl trends evaluated from ACE-FTS, TOMCAT and TCOM datasets averaged between 28.5 and 48.5 km in altitude and 60°S to 60°N latitude.

Table 3. CFC-11 trends from Schmidt et al. (2024) and calculated from ACE-FTS, TOMCAT and TCOM datasets using the method illustrated in Section 2.1.

	Slope 2005-2014 [ppt/yr]	Slope 2015-2019 [ppt/yr]	Slope 2019-2024 [ppt/yr]
ACE v5.2 (Schmidt)	-1.89 ± 0.02	-1.00 ± 0.05	-2.12 ± 0.06
NOAA NH (Schmidt)	-2.07 ± 0.01	-1.03 ± 0.01	-2.74 ± 0.04
ACE v5.2	-1.75 ± 0.01	-1.41 ± 0.07	-2.34 ± 0.05
TOMCAT	-1.93 ± 0.01	-1.15 ± 0.02	-1.83 ± 0.01
TCOM	-1.88 ± 0.01	-1.14 ± 0.02	-2.05 ± 0.02

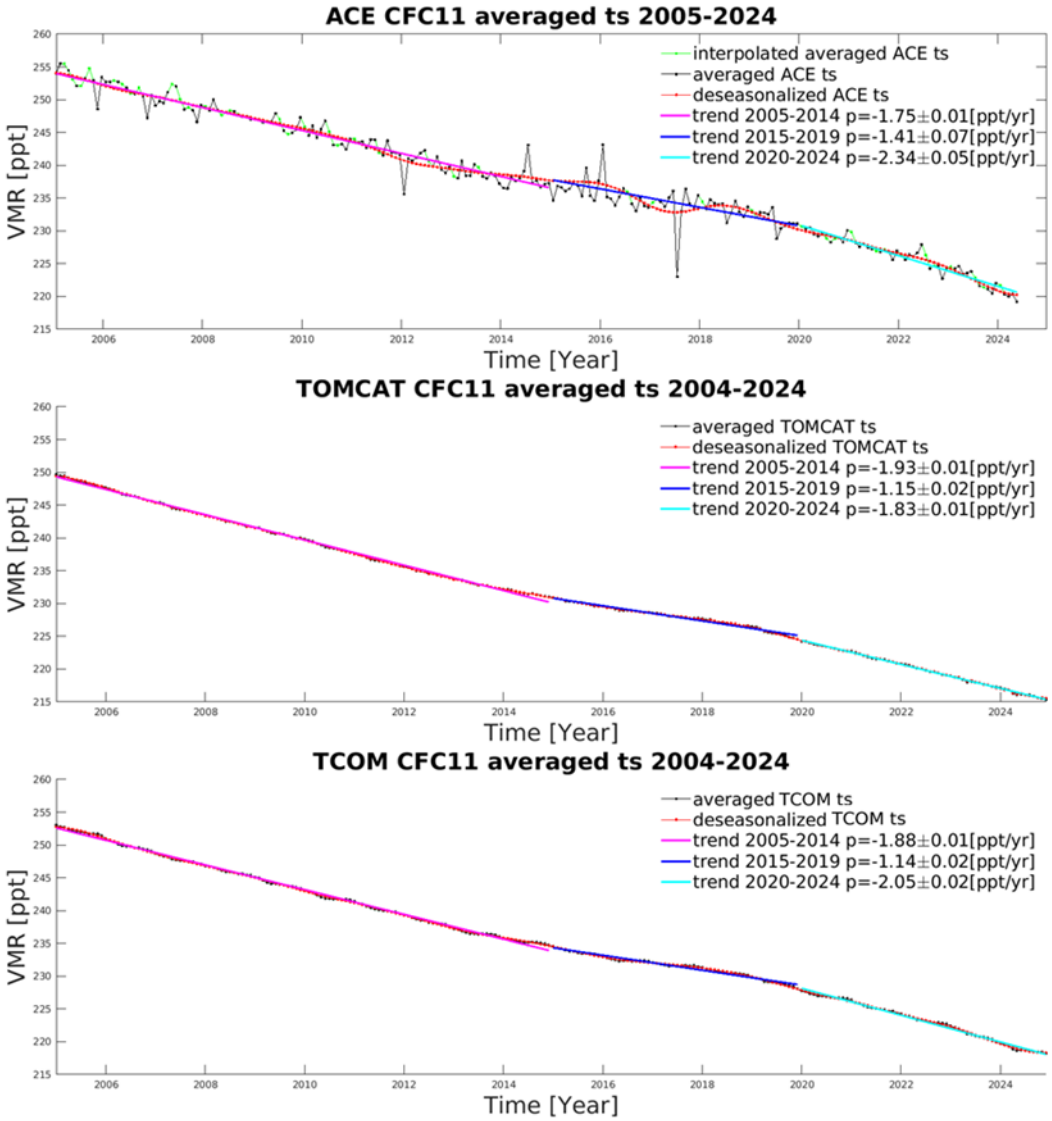

Figure 5. CFC-11 trends evaluated from ACE-FTS, TOMCAT and TCOM datasets averaged between 17.5 km and 28.5 km in altitude and 30°S to 30°N latitude.

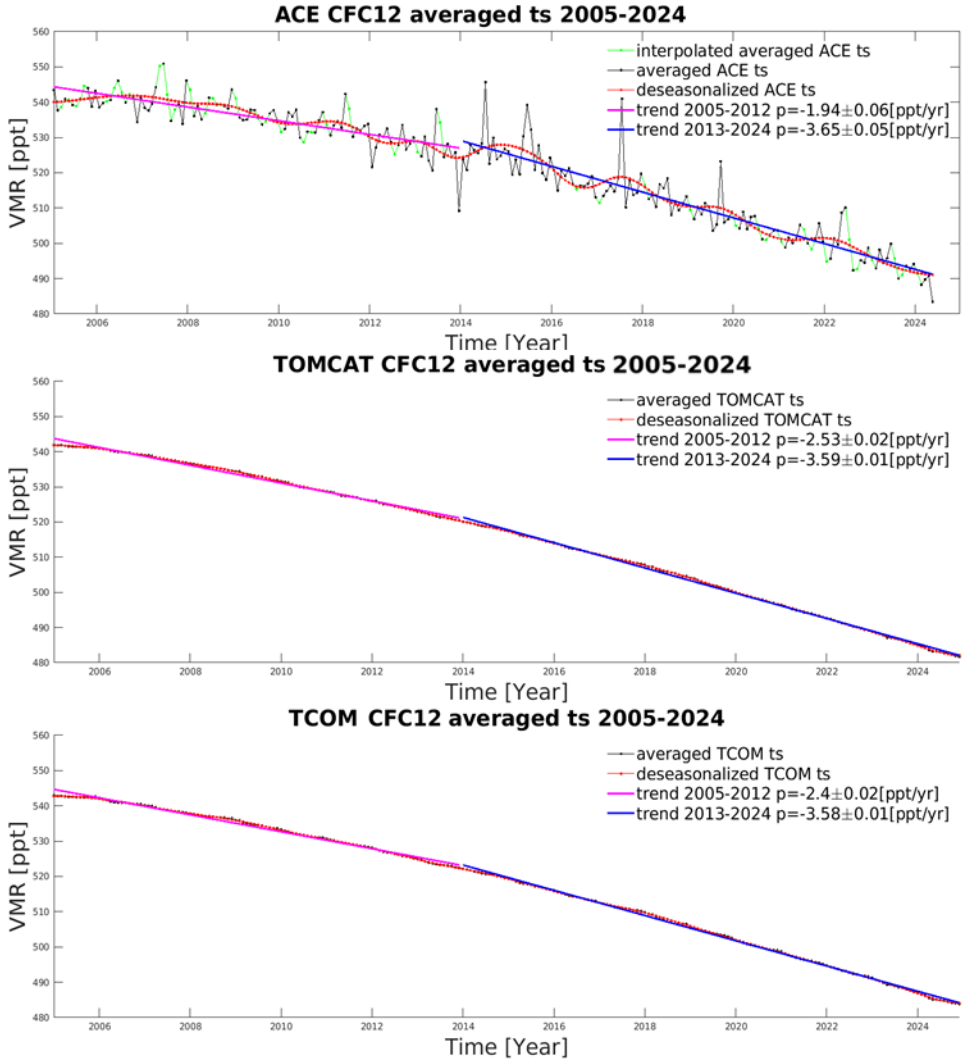

Figure 6. CFC-12 trends evaluated from ACE-FTS, TOMCAT and TCOM datasets averaged between 17.5 km and 28.5 km in altitude and 30°S to 30°N latitude.

Table 4. CFC-12 trends from Schmidt et al. (2024) and calculated from ACE-FTS, TOMCAT and TCOM datasets using the method illustrated in Section 2.1.

	Slope 2005-2012 [ppt/yr]	Slope 2013-2024 [ppt/yr]
ACE v5.2 (Schmidt)	-1.44 ± 0.08	-3.16 ± 0.04
NOAA NH (Schmidt)	-1.47 ± 0.05	-3.20 ± 0.02
ACE v5.2	-1.94 ± 0.06	-3.65 ± 0.05
TOMCAT	-2.53 ± 0.02	-3.59 ± 0.01
TCOM	-2.40 ± 0.02	-3.58 ± 0.01

3.3 Nonlinear trends

The EMD residuals (Figure 7) allow us to investigate the nonlinear trend in the zonal means by calculating their first derivatives. The calculated rates for both ACE-FTS and TCOM HCl datasets show an anomalous enhancement in the rate of decrease between 40°S and 50°S over the period 2020-2022, as highlighted by red circles in Figure 8. Data gaps and artifacts introduced by the interpolation process result in more variability in the ACE time series, reducing the detectability of these anomalous decreases. Moreover, the methodology employed quantifies local variability and is consequently highly sensitive to rapid temporal variations in the time series. The feature circled in red is believed to be associated with the 2020 Australian wildfires emissions that reduced the HCl amount in the region (Santee et al., 2022). Further investigation on the robustness of the methodology and on the data are necessary to assess this hypothesis.

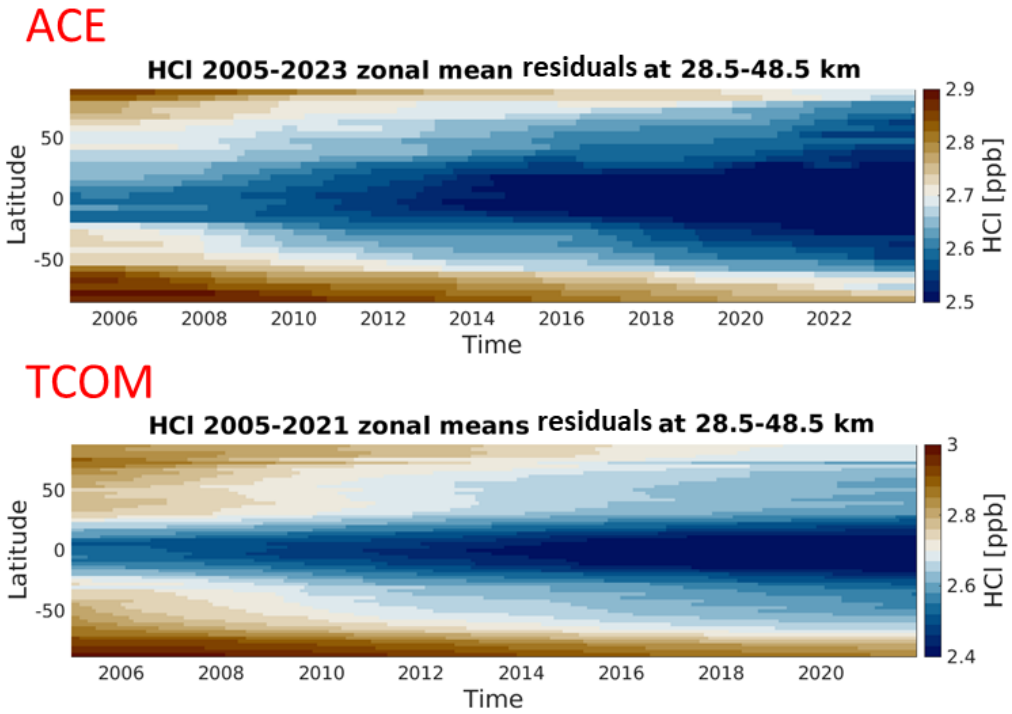

Figure 7. HCl EMD residuals from ACE-FTS observations (top panel) and TCOM data (bottom panel).

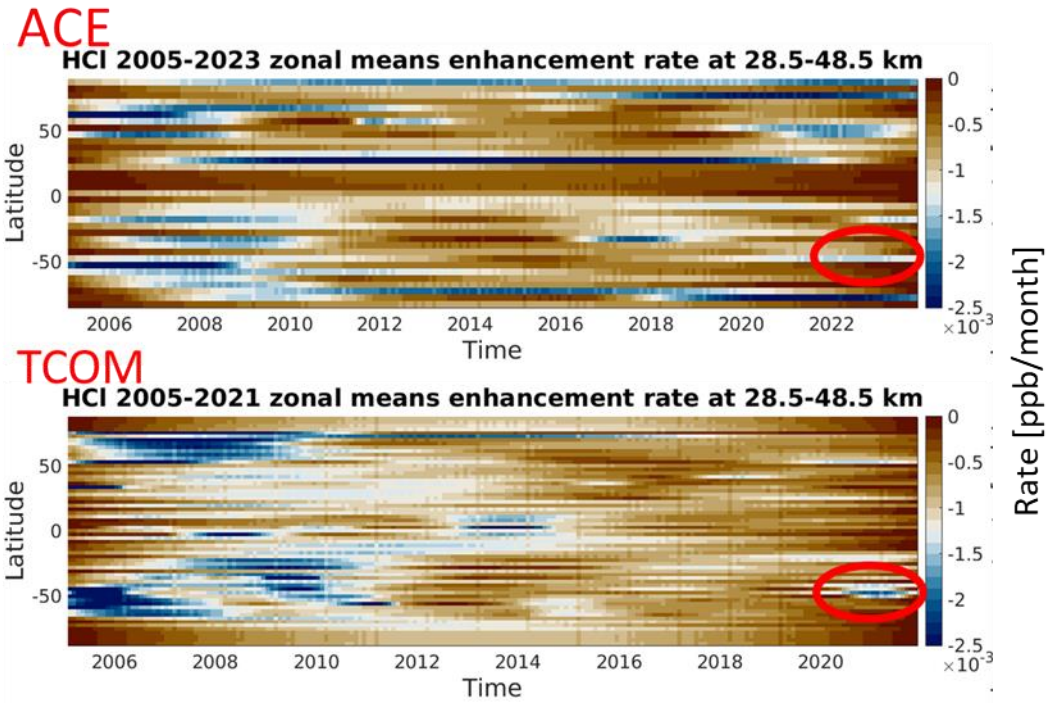

Figure 8. First derivative of the HCl residuals from ACE-FTS (top panel) and TCOM (bottom panel). Red circles highlight the anomalous decreasing rates possibly associated with the 2020 Australian wildfires.

3.4 Bespoke TOMCAT model calculations

To assess the influence of the Montreal Protocol in successfully reducing emissions of ozone-depleting species, we used TOMCAT model simulations to evaluate HCl, the main Cl reservoir species. Two configurations were considered: a control run reproducing the observed decline in chlorine, and a bespoke run with chlorine source gas concentrations fixed to their peak 1995 values.

Figures Figure 9 and Figure 10 present, respectively, the global HCl trends and the trends averaged over the region spanning 28.5–48.5 km in altitude and 60°S–60°N in latitude for both TOMCAT simulations. The control run reproduces the expected HCl trends associated with decreasing halocarbon emissions, while the constant-Cl simulation shows a small increase in HCl globally, becoming larger in the northern hemisphere below 25 km, consistent with increasing stratospheric ozone loss. Figure 9 highlights the spatial pattern of HCl reduction between 2005 and 2021, and Figure 10 illustrates the corresponding mean trends, emphasizing the stronger decline in the real world.

Together, these simulations demonstrate the TOMCAT model's strong sensitivity of stratospheric chlorine loading to source gas emissions. The comparison between the control and constant-Cl runs confirms that changes in chlorine source gas concentrations directly influence the modeled HCl trends: when chlorine levels decrease, TOMCAT reproduces the expected negative trends, whereas fixing chlorine to 1995 peak values results in positive trends in HCl. TOMCAT captures the chemical response of the stratosphere to halocarbon source gas decline, and can also be used to show us a world in the absence of the Montreal Protocol, albeit with source gas concentrations fixed to 1995 values. The increasing HCl concentrations of the bespoke model run are linked to increasing stratospheric ozone loss.

TOMCAT results can therefore be used as a reference for atmospheric halocarbon monitoring by quantifying the expected trends under known chlorine conditions, and setting expectations for ozone recovery. This work shows the value of limb sounders like ACE-FTS, which measures both source and product chlorine species, in support of the Montreal Protocol.

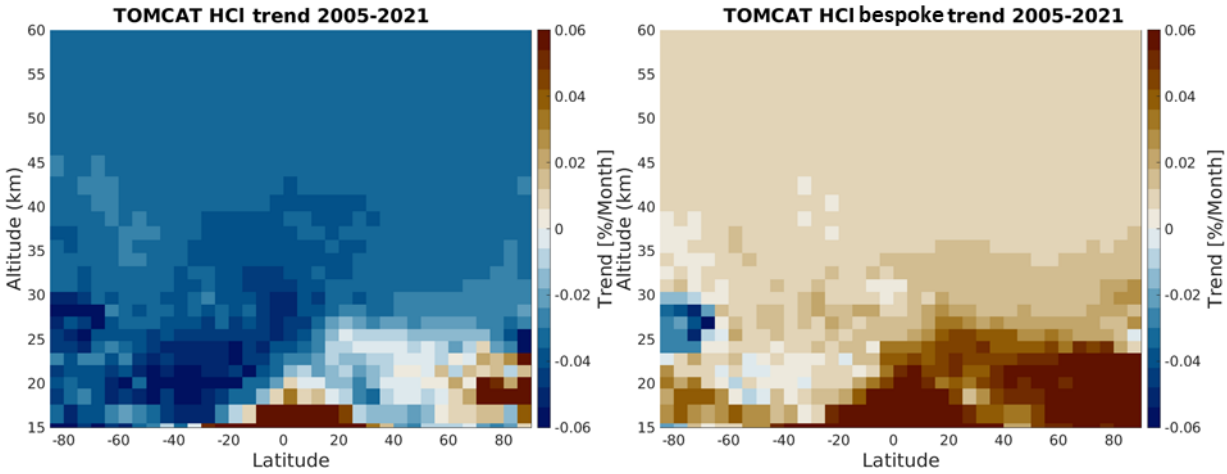

Figure 9. Cross-sectional HCl trends between 2005 and 2021 for TOMCAT control run (left), TOMCAT bespoke model run with constant Cl at peak 1995 values (right).

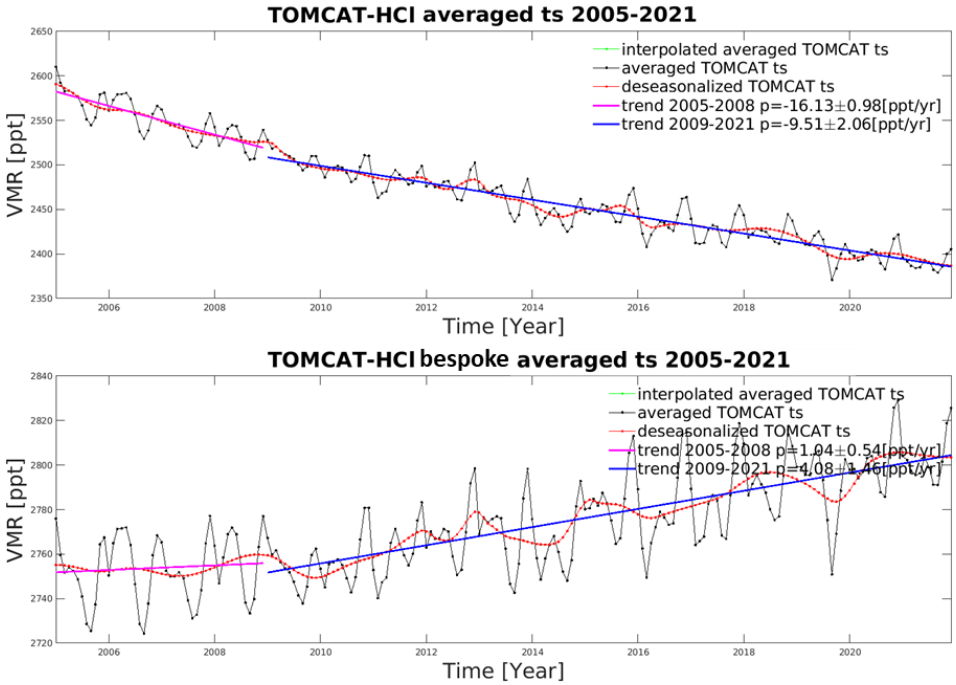

Figure 10. HCl trends evaluated from TOMCAT control and bespoke model runs, with constant Cl at peak (1995) values, averaged between 28.5 and 48.5 km in altitude and 60°S to 60°N latitude.

4 Outlook and Future work

There are several possibilities for further developing the present work in future studies:

- **Extension of the ACE-FTS observational record:** ACE-FTS is continuing to operate well beyond its original design lifetime. As long as observations are maintained, the analysis described here can be extended temporally. The resulting longer time series will enable a more robust separation of natural variability from long-term trends.
- **Integration of additional satellite limb datasets:** The trends presented here are primarily derived from ACE-FTS observations. Future work could incorporate data from other satellite limb sensors, including instruments that overlap with ACE-FTS but provide broader spatial coverage, such as the Microwave Limb Sounder (MLS), as well as earlier missions that extend the observational record to prior periods, such as the Halogen Occultation Experiment (HALOE). Careful consideration will be required to address potential biases between the datasets.
- **Expansion to additional minor gases:** The current trend analysis based on ACE-FTS, TOMCAT, and TCOM could be expanded through the construction of additional minor-gas datasets, including HF, CFC-113, HCFC-141b, HCFC-142b, HFC-134a, HCFC-22, and OCS. This would broaden the scope of the study and improve the representation of halogenated and related species in the atmosphere.
- **Assessment of contributions from Very Short-Lived Substances (VSLS):** An overarching aim of this work is to assess the success of the Montreal Protocol. One potential challenge for the Protocol is the increased stratospheric loading of chlorine derived from Very Short-Lived Substances (VSLS). Such contributions would be reflected in HCl trends, the major chlorine reservoir, that differ from expectations based solely on long-lived chlorine source gases. Detailed comparisons between HCl and source-gas trends could therefore provide insight into this contribution.
- **Use of complementary tracers to diagnose circulation changes:** Trends in complementary long-lived source gases such as CH_4 and N_2O can provide valuable information on variability and long-term changes in stratospheric circulation. Incorporating these tracers would allow improved attribution of observed trends in chlorine-containing species and their relationship to reductions in surface emissions.
- **Preparation for potential observational gaps:** In the longer term, an observational gap in satellite limb measurements of stratospheric chlorine profiles is likely. In such a scenario, extensions of machine-learning approaches, such as those used in the ML-TOMCAT and TCOM datasets, combined with surface network observations (e.g., the Network for the Detection of Atmospheric Composition Change), nadir-sounding instruments, and 3-D modelling, could provide an important reconstruction of optimal profile datasets. Development of these methodologies should therefore continue while ACE-FTS is still operational.
- **Development of neural-network–based frameworks:** Further methodological improvements could include the development of neural-network approaches to generate machine-learning–based datasets similar to TCOM. This would support a consistent analytical framework across multiple species and facilitate more uniform comparisons between observational and model-derived products.
- **Comparison with surface monitoring observations:** Finally, future work could involve comparing total column changes derived from these datasets with measurements from surface monitoring sites. Such comparisons would help evaluate the robustness of the calculated trends, assess the consistency between column-integrated and surface observations, and improve confidence in long-term trend estimates.

List of acronyms and abbreviations

ACE-FTS	Atmospheric Chemistry Experiment – Fourier Transform Spectrometer
CCI	Climate Change Initiative
CFC	Chlorofluorocarbons
ECMWF	European Centre for Medium-Range Weather Forecasts
ECV	Essential Climate Variable
EMD	Empirical Mode Decomposition
ESA	European Space Agency
GHG	Greenhouse Gas
HALOE	HALogen Occultation Experiment
HCl	Hydrogen Chloride
HCFC	Hydrochlorofluorocarbons
HF	Hydrogen Fluoride
HFC	Hydrofluorocarbons
IMFs	Intrinsic Mode Functions
LOLIPOP	Long Lived greenhouse gas PrOducts Performances
ML	Machine Learning
MP	Montreal Protocol
ODS	Ozone-Depleting Substance
XGBoost	eXtreme Gradient Boost

References

Bernath, P.F., 2017. The Atmospheric Chemistry Experiment (ACE). J. Quant. Spectrosc. Radiat. Transf. 186, 3–16. https://doi.org/10.1016/j.jqsrt.2016.04.006

Bernath, P.F., 2005. Atmospheric Chemistry Experiment (ACE): Mission overview, in: Fourier Transform Spectroscopy/ Hyperspectral Imaging and Sounding of the Environment. Presented at the Fourier Transform Spectroscopy, OSA, Alexandria, Virginia, p. JMA3. https://doi.org/10.1364/FTS.2005.JMA3

Boone, C.D., Bernath, P.F., Lecours, M., 2023. Version 5 retrievals for ACE-FTS and ACE-imagers. J. Quant. Spectrosc. Radiat. Transf. 310, 108749. https://doi.org/10.1016/j.jqsrt.2023.108749

Chipperfield, M.P., Dhomse, S., Hossaini, R., Feng, W., Santee, M.L., Weber, M., Burrows, J.P., Wild, J.D., Loyola, D., Coldewey-Egbers, M., 2018. On the Cause of Recent Variations in Lower Stratospheric Ozone. Geophys. Res. Lett. 45, 5718–5726. https://doi.org/10.1029/2018GL078071

Colominas, M.A., Schlotthauer, G., Torres, M.E., 2014. Improved complete ensemble EMD: A suitable tool for biomedical signal processing. Biomed. Signal Process. Control 14, 19–29. https://doi.org/10.1016/j.bspc.2014.06.009

Dhomse, S., 2026a. TCOM-CFC11 : TOMCAT CTM and Occultation Mesurement based CFC-11 profile data set. https://doi.org/10.5281/ZENODO.18145730

Dhomse, S., 2026b. TCOM-CFC12 : TOMCAT CTM and Occultation measurement-based CFC12 profile data set. https://doi.org/10.5281/ZENODO.18147392

Dhomse, S., 2026. TCOM-HCl : TOMCAT CTM and Occultation Measurements based HCl profile data set. https://doi.org/10.5281/ZENODO.18184430

Dhomse, S., Chipperfield, M.P., 2026. TCOM-CFC11 and TCOM-CFC12: A Gap-Free, Observationally Constrained Global Dataset of Stratospheric CFC-11 and CFC-12 Profiles (v2.0). Earth Syst. Sci. Data. https://doi.org/Submitted

Dhomse, S.S., Chipperfield, M.P., 2023. Using machine learning to construct TOMCAT model and occultation measurement-based stratospheric methane (TCOM-CH4) and nitrous oxide (TCOM-N2O) profile data sets. Earth Syst. Sci. Data 15, 5105–5120. https://doi.org/10.5194/essd-15-5105-2023

Feng, W., Dhomse, S.S., Arosio, C., Weber, M., Burrows, J.P., Santee, M.L., Chipperfield, M.P., 2021. Arctic Ozone Depletion in 2019/20: Roles of Chemistry, Dynamics and the Montreal Protocol. Geophys. Res. Lett. 48, e2020GL091911. https://doi.org/10.1029/2020GL091911

Hossaini, R., Chipperfield, M.P., Montzka, S.A., Rap, A., Dhomse, S., Feng, W., 2015. Efficiency of short-lived halogens at influencing climate through depletion of stratospheric ozone. Nat. Geosci. 8, 186–190. https://doi.org/10.1038/ngeo2363

Huang, N.E., Shen, Z., Long, S.R., Wu, M.C., Shih, H.H., Zheng, Q., Yen, N.-C., Tung, C.C., Liu, H.H., 1998. The empirical mode decomposition and the Hilbert spectrum for nonlinear and non-stationary time series analysis. Proc. R. Soc. Lond. Ser. Math. Phys. Eng. Sci. 454, 903–995. https://doi.org/10.1098/rspa.1998.0193

Li, H., Wang, Y., Ma, Y., 2010. Ensemble empirical mode decomposition and Hilbert-Huang transform applied to bearing fault diagnosis, in: 2010 3rd International Congress on Image and Signal Processing. Presented at the 2010 3rd International Congress on Image and Signal Processing (CISP), IEEE, Yantai, China, pp. 3413–3417. https://doi.org/10.1109/CISP.2010.5647389

Mahieu, E., Chipperfield, M.P., Notholt, J., Reddmann, T., Anderson, J., Bernath, P.F., Blumenstock, T., Coffey, M.T., Dhomse, S.S., Feng, W., Franco, B., Froidevaux, L., Griffith, D.W.T., Hannigan, J.W., Hase, F., Hossaini, R., Jones, N.B., Morino, I.,

Murata, I., Nakajima, H., Palm, M., Paton-Walsh, C., Iii, J.M.R., Schneider, M., Servais, C., Smale, D., Walker, K.A., 2014. Recent Northern Hemisphere stratospheric HCl increase due to atmospheric circulation changes. Nature 515, 104–107. https://doi.org/10.1038/nature13857

Montzka, S.A., Dutton, G.S., Yu, P., Ray, E., Portmann, R.W., Daniel, J.S., Kuijpers, L., Hall, B.D., Mondeel, D., Siso, C., Nance, J.D., Rigby, M., Manning, A.J., Hu, L., Moore, F., Miller, B.R., Elkins, J.W., 2018. An unexpected and persistent increase in global emissions of ozone-depleting CFC-11. Nature 557, 413–417. https://doi.org/10.1038/s41586-018-0106-2

Santee, M.L., Lambert, A., Manney, G.L., Livesey, N.J., Froidevaux, L., Neu, J.L., Schwartz, M.J., Millán, L.F., Werner, F., Read, W.G., Park, M., Fuller, R.A., Ward, B.M., 2022. Prolonged and Pervasive Perturbations in the Composition of the Southern Hemisphere Midlatitude Lower Stratosphere From the Australian New Year's Fires. Geophys. Res. Lett. 49, e2021GL096270. https://doi.org/10.1029/2021GL096270

Schmidt, M., Bernath, P., Boone, C., Lecours, M., Steffen, J., 2024. Trends in atmospheric composition between 2004–2023 using version 5 ACE-FTS data. J. Quant. Spectrosc. Radiat. Transf. 325, 109088. https://doi.org/10.1016/j.jqsrt.2024.109088

Stallone, A., Cicone, A., Materassi, M., 2020. New insights and best practices for the successful use of Empirical Mode Decomposition, Iterative Filtering and derived algorithms. Sci. Rep. 10, 15161. https://doi.org/10.1038/s41598-020-72193-2

Torres, M.E., Colominas, M.A., Schlotthauer, G., Flandrin, P., 2011. A complete ensemble empirical mode decomposition with adaptive noise, in: 2011 IEEE International Conference on Acoustics, Speech and Signal Processing (ICASSP). Presented at the ICASSP 2011 - 2011 IEEE International Conference on Acoustics, Speech and Signal Processing (ICASSP), IEEE, Prague, Czech Republic, pp. 4144–4147. https://doi.org/10.1109/ICASSP.2011.5947265

World Meteorological Organization, 2023. State of the Global Climate 2022. United Nations, Erscheinungsort nicht ermittelbar.

***** End of Document *****